Pt nanoparticles modified on ultrathin $Ni(OH)_2$ nanosheets for enhanced seawater urea electro-oxidation and hydrogen evolution at industrial-grade current density

Jie Tian, Shiyu Wang, Min Wang, Nana Zheng, Jing Xie, Jindou Hu, Zhenjiang Lu*, Yali Cao*

State Key Laboratory of Chemistry and Utilization of Carbon Based Energy Resources, College of Chemistry, Xinjiang University, Urumqi 830017, Xinjiang, PR China

*Corresponding authors.

E-mails: caoyali523@163.com (Yali Cao); luzj@xju.edu.cn (Zhenjiang Lu).

Experiment

Materials

Foam nickel (NF) was purchased from Suzhou Zhengtairong New Material Co., LtD. The Hydroxide potassium (KOH) and chloroplatinic acid (H_2PtCl_6) were purchased from Aladdin (Shanghai). Nafion (5 wt%) was supplied from Energy Chemica Co., Ltd. Commercial platinum carbon (Pt/C, AR, 20%) were obtained by Suzhou Yilongsheng Energy Technology Co., Ltd. Anhydrous ruthenium oxide (RuO_2, AR, 99.7 %) was purchased from Alfa Aesar. The seawater sample was collected from the Bohai Sea (Huludao City, Liaoning Province) in China.

Fabrication of Pt/Ni(OH)$_2$/NF

First, 3 mL of H_2PtCl_6 (0.2 M) solution was dispensed into a certain amount of DI water, and the solution was then subjected to intense stirring. Subsequently, the cleaned NF (2.5 × 4 cm^2, thickness: 1 mm) was relocated into the mixed solution for 3 h. Following the completion of the reaction, the NF was subjected to a rinse using DI water and absolute ethanol, and then desiccated under vacuum for 10 h. The as-prepared sample is named Pt/Ni(OH)$_2$/NF. Subsequent to modifying the reaction time to 2 h and 4 h, Pt/Ni(OH)$_2$/NF-2h and Pt/Ni(OH)$_2$/NF-4h were obtained respectively.

Synthesis of Pt/NF

Firstly, the Pt/Ni(OH)$_2$/NF was immersed in 1 M HCl for a duration of 3 h. Subsequently, the sample washed with deionized water and ethanol, followed by vacuum drying at 60℃ for 10 h. Finally, Pt/NF was prepared.

Preparation commercial Pt/C/NF and RuO_2/NF

2.5 mg of Pt/C or RuO_2 were each introduced separately into 500 μL of a mixture (deionized water: isopropanol: Nafion = 245 μL : 245 μL : 10 μL), followed by ultrasonication for 30 minutes to prepare an ink with homogeneous dispersion. 20 μL of the dispersed solution was slowly dripped onto the pre-cleaned nickel foam, followed by drying at 60℃ to yield the electrodes.

Characterization

The crystal structures of the catalysts were acquired utilizing an X - ray diffractometer (XRD, Bruker D8 ADVANCE). The morphological characteristics and nanostructural features of the catalysts were examined using scanning electron microscopy (SEM, Hitachi S-4800H), transmission electron microscopy (TEM, Hitachi-600), and high-resolution transmission electron microscopy (HRTEM, JEOL JEM-2010F). The concentration of Pt within the Pt/Ni(OH)$_2$/NF composite was determined through inductively coupled plasma optical emission spectroscopy (ICP-OES, Optima 8000). The elemental makeup and chemical oxidation states were ascertained through X - ray photoelectron spectroscopy (XPS). The work function was determined by means of ultraviolet photoelectron spectroscopy (UPS).

Electrochemical characterizations

The HER and UOR performance evaluations were conducted utilizing a three-electrode setup on an electrochemical workstation (Chenhua CHI760E, Shanghai). A standard three-electrode configuration was assembled, with the reference electrode (RE) being Hg/HgO, the counter electrode made of platinum wire, and the working electrode comprising the as-synthesized catalyst. The potential measurement was adjusted to the reversible hydrogen electrode (RHE) scale through the Nernst equation ($E_{RHE} = E_{Hg/HgO}$ + 0.098 V + 0.059 pH). To evaluate the activity of the catalysts with respect to the hydrogen evolution reaction (HER) and oxygen evolution reaction (OER), linear sweep voltammetry (LSV) curves were generated at a scan rate of 5 mV s^{-1}. These curves were subsequently employed to construct Tafel plots. For the polarization curves of OER and HER, the iR values are subjected to manual correction according to the subsequent equation:

$$E_{RHE} = E_{Hg/HgO} + 0.098\ V + 0.059\ pH\text{-}iR_s$$

(where R_s is the solution resistance, i is the corresponding current).

The electrochemical double-layer capacitance (C_{dl}) of the as-synthesized catalysts was determined through cyclic voltammetry (CV) curves within the non-Faradaic region at scan rates spanning from 10 to 120 mV s^{-1}. The value of the electrochemically

active surface area (ECSA) is calculated according to CV. Electrochemical impedance spectroscopy (EIS) data were collected at different potentials within a frequency range from 100 kHz to 10 mHz. Furthermore, to assess the catalytic performance for overall water splitting (OWS), an experiment utilizing a two-electrode system was conducted. The stability of HER, UOR, and OWS was determined by chronopotentiometry.

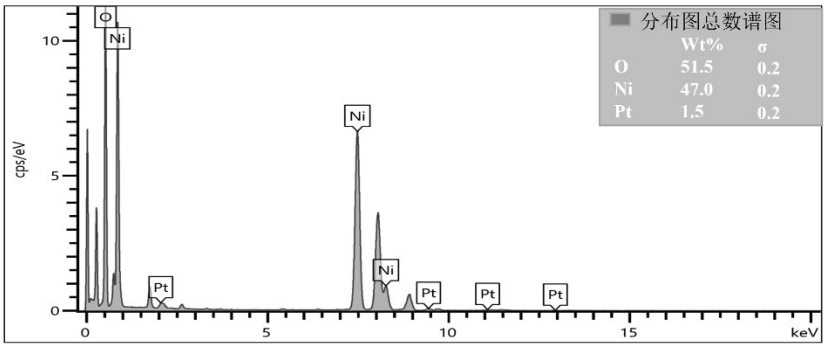

Fig. S1 The energy dispersive spectroscopy (EDS) test of Pt/Ni(OH)$_2$/NF.

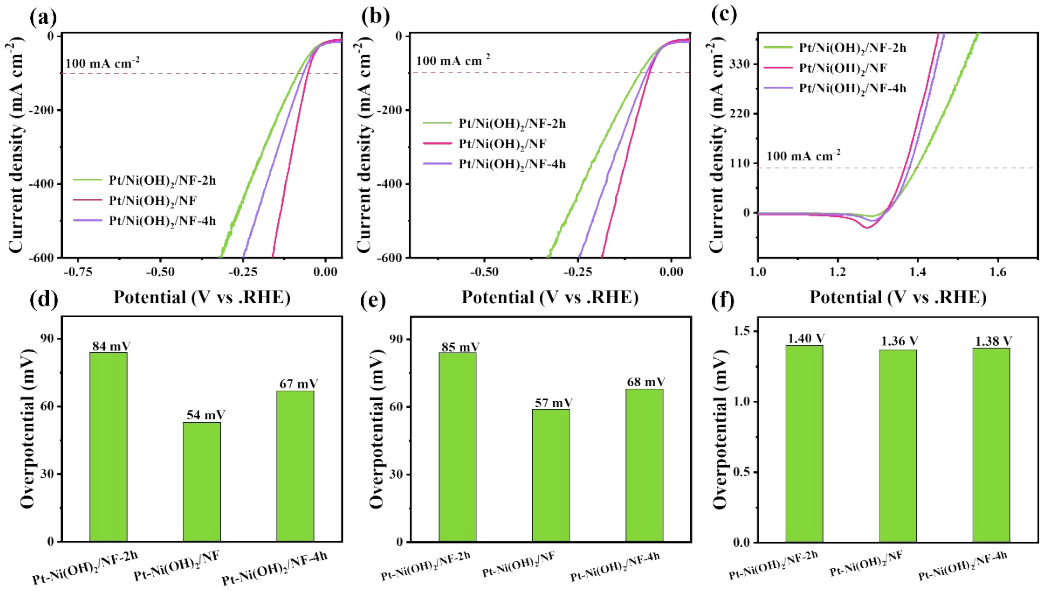

Fig. S2 (a, d) HER LSV curves and overpotential in 1 M KOH. (b, e) HER LSV curves and overpotential in 1 M KOH + 0.5 M urea. (c, f) UOR LSV curves and overpotential in 1 M KOH + 0.5 M urea of the samples with different reaction times.

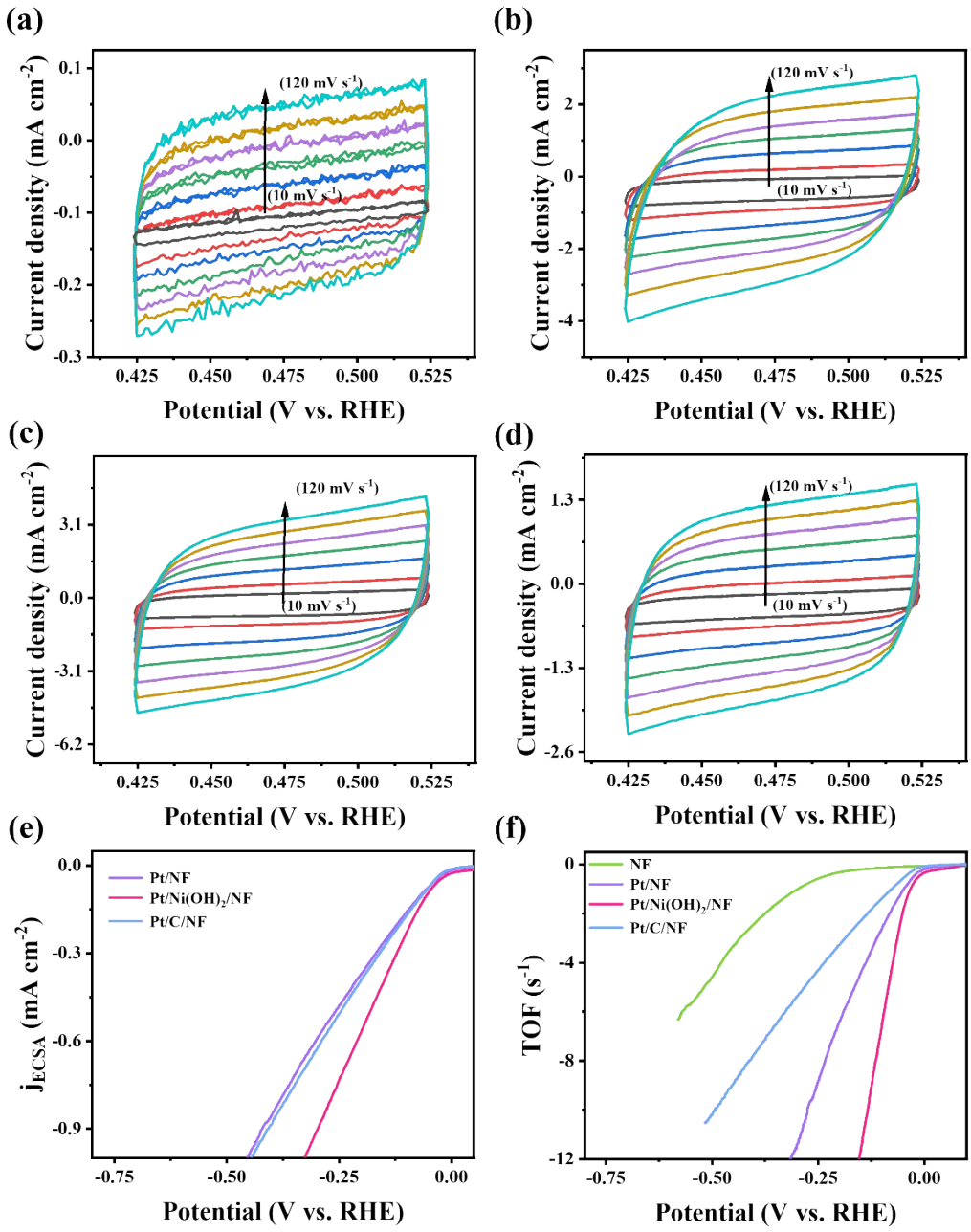

Fig. S3 The different sweep CV curves in the non-Faraday interval of (a) NF, (b) Pt/NF, (c) Pt/Ni(OH)$_2$/NF and (d) Pt/C/NF. (e) ECSA normalized for the current density curves and (f) TOF values of the different samples in 1 M KOH.

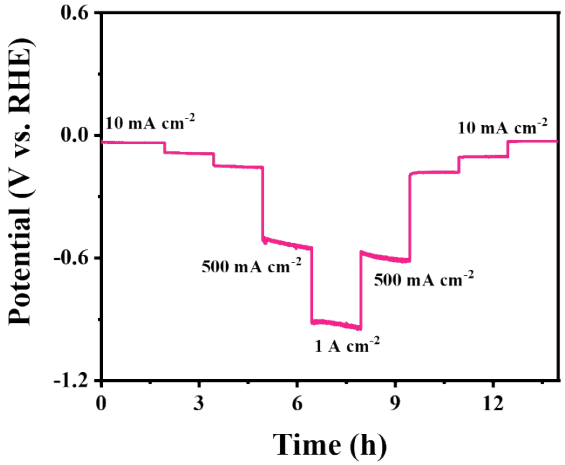

Fig. S4 The multi-step chronoamperometry tests of Pt/Ni(OH)$_2$/NF in 1 M KOH.

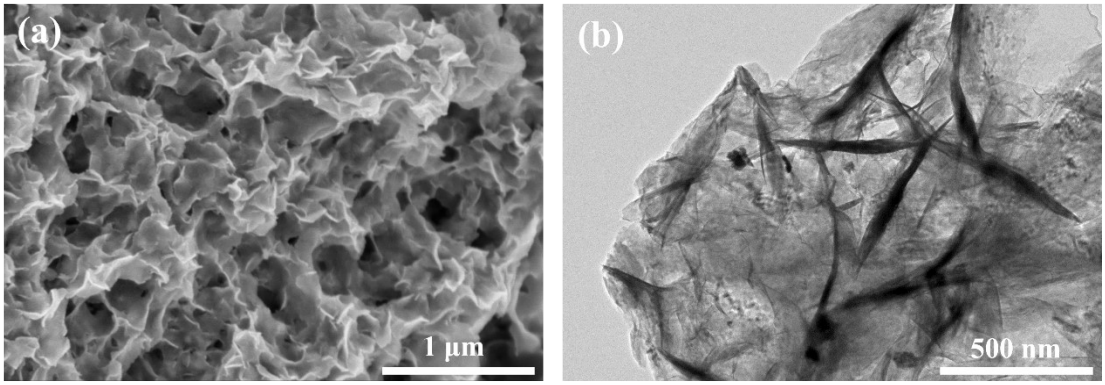

Fig. S5 (a) SEM diagram and (b) TEM diagram after stability test of Pt/$Ni(OH)_2$/NF in 1 M KOH.

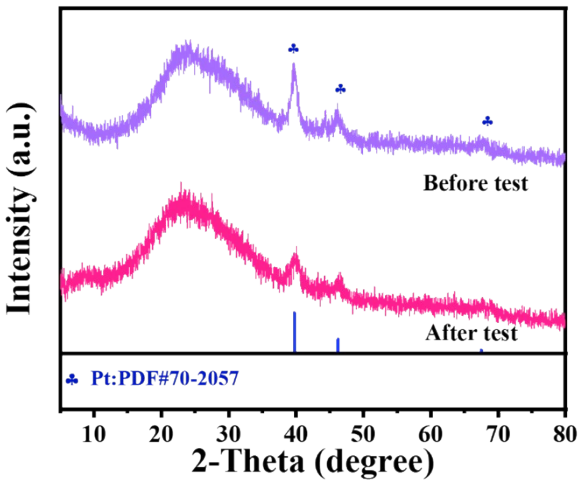

Fig. S6 XRD diagram before and after stability test for Pt/Ni(OH)$_2$/NF in 1 M KOH.

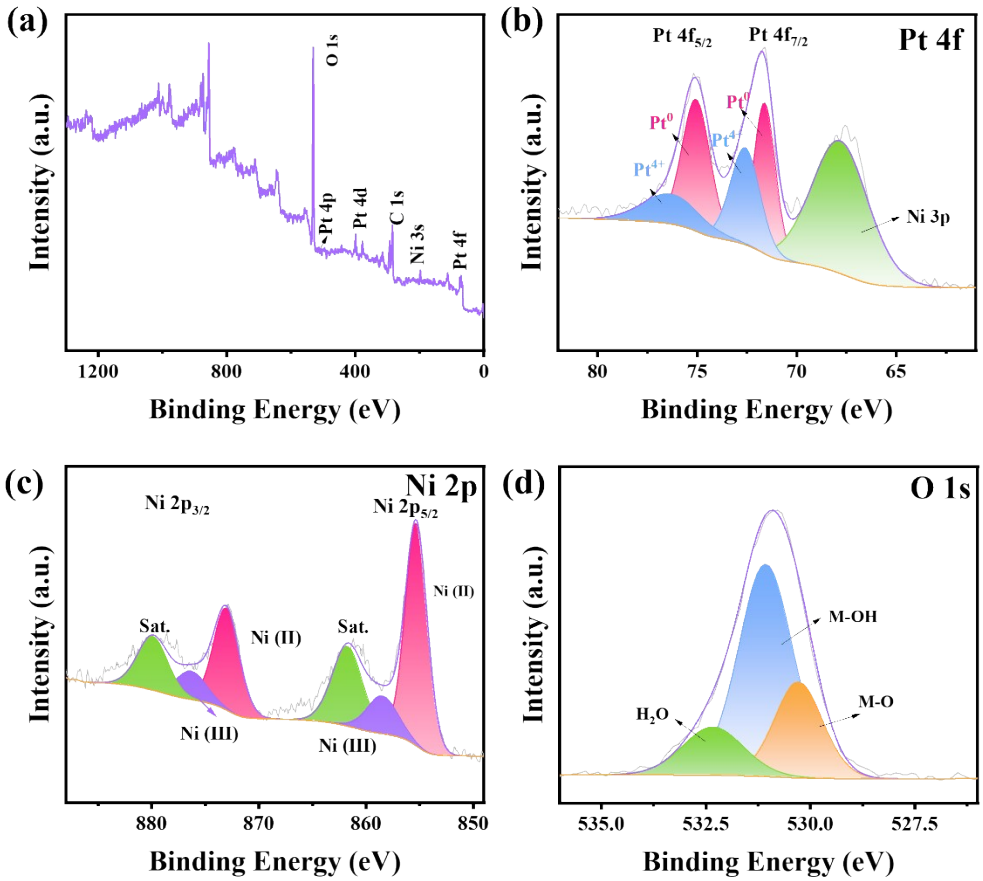

Fig. S7 XPS spectra of (a) full spectrum, (b) Pt 4f, (c) Ni 2p, and (d) O 1s of as-obtained samples after stability test for Pt/Ni(OH)$_2$/NF.

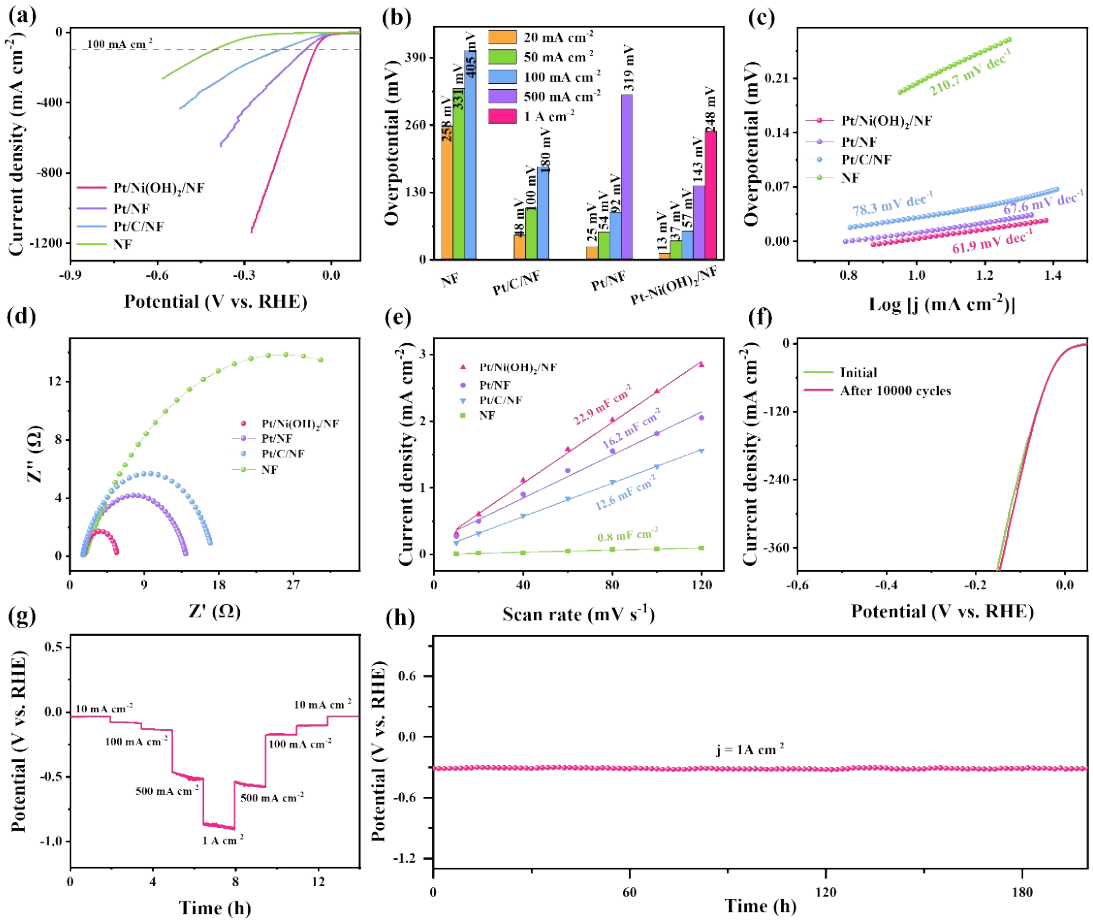

Fig. S8 (a) LSV polarization curves, (b) Overpotentials, (c) Tafel slopes plots, (d) Electrochemical impedance spectroscopy (EIS) test, and (e) C_{dl} of as-prepared catalysts. (f) LSV curves after 10000 cycles, (g) The multi-step chronoamperometry tests, and (h) Chronopotentiometric test at 1 A cm^{-2} of $Pt/Ni(OH)_2/NF$.

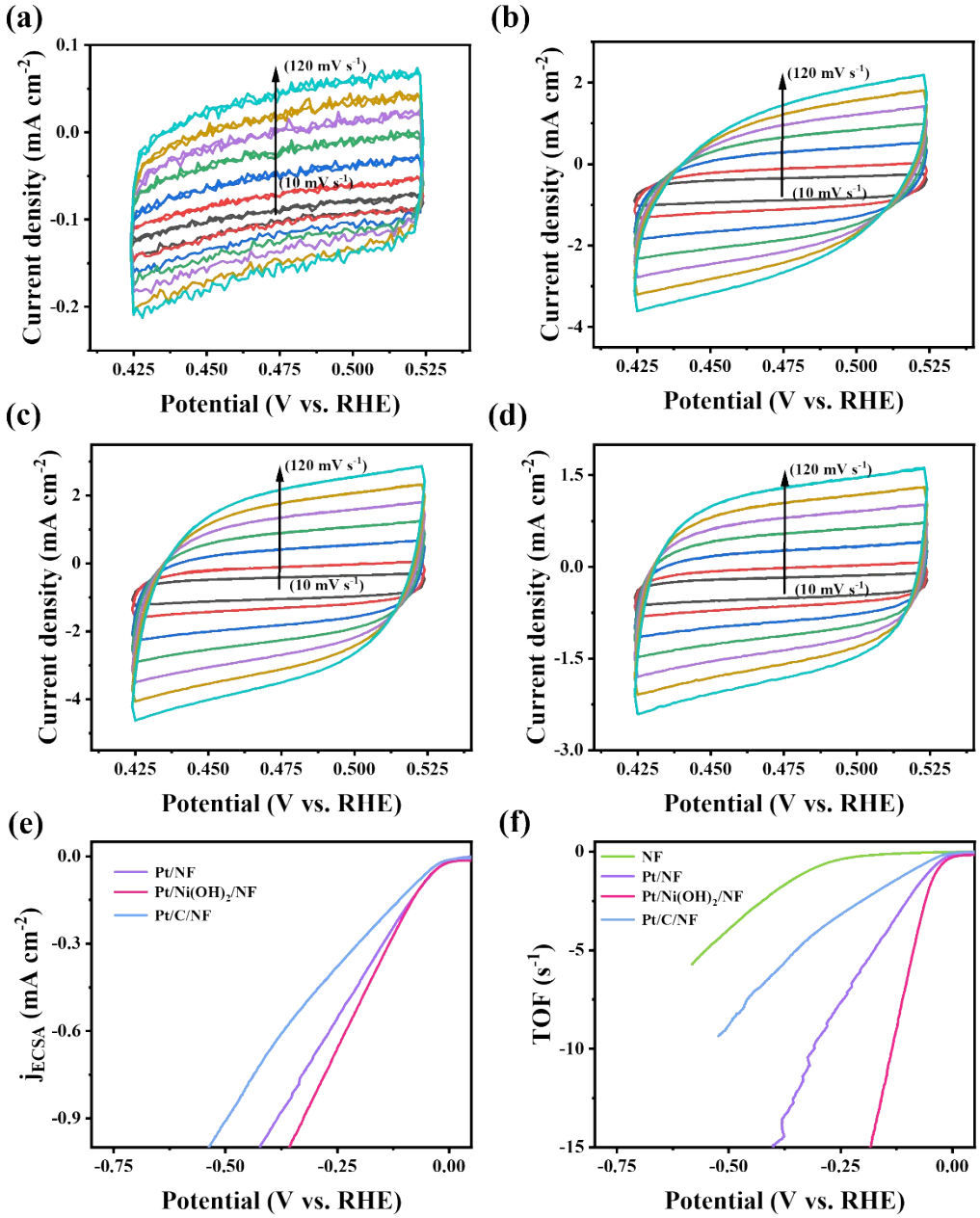

Fig. S9 The different sweep CV curves in the non-Faraday interval of (a) NF, (b) Pt/NF, (c) Pt/Ni(OH)$_2$/NF and (d) Pt/C/NF. (e) ECSA normalized for the current density curves and (f) TOF values of the different samples in 1 M KOH + 0.5 M urea.

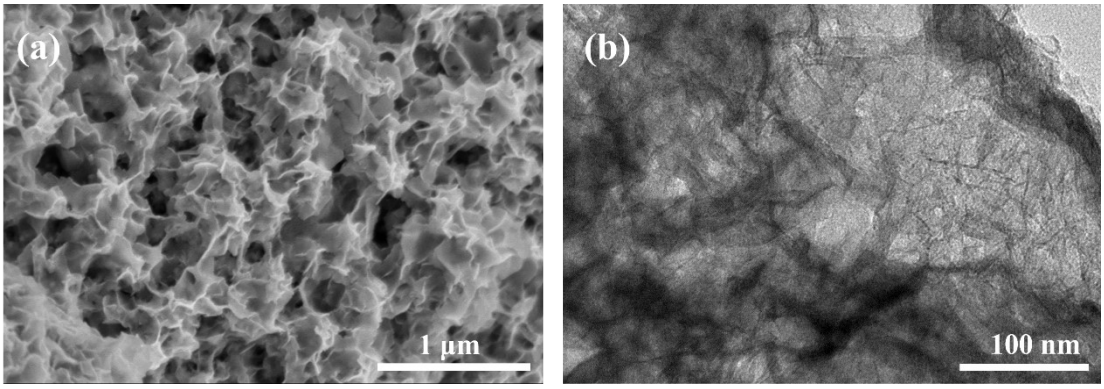

Fig. S10 (a) SEM diagram and (b) TEM diagram after stability test of Pt/$Ni(OH)_2$/NF in 1 M KOH + 0.5 M urea.

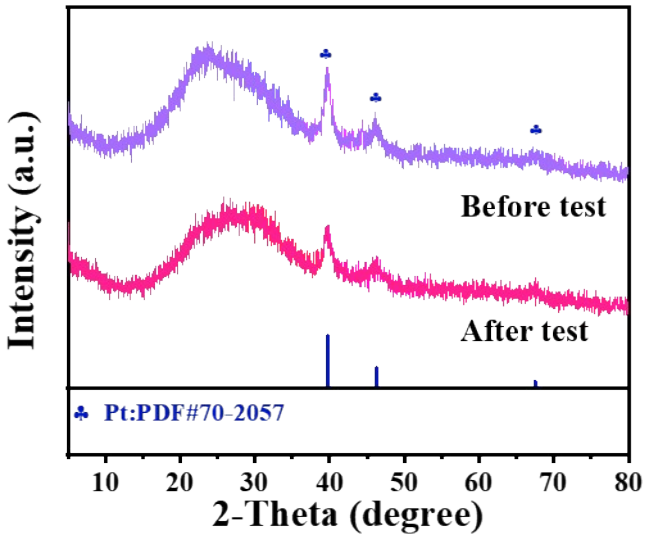

Fig. S11 XRD diagram before and after stability test for Pt/Ni(OH)$_2$/NF.

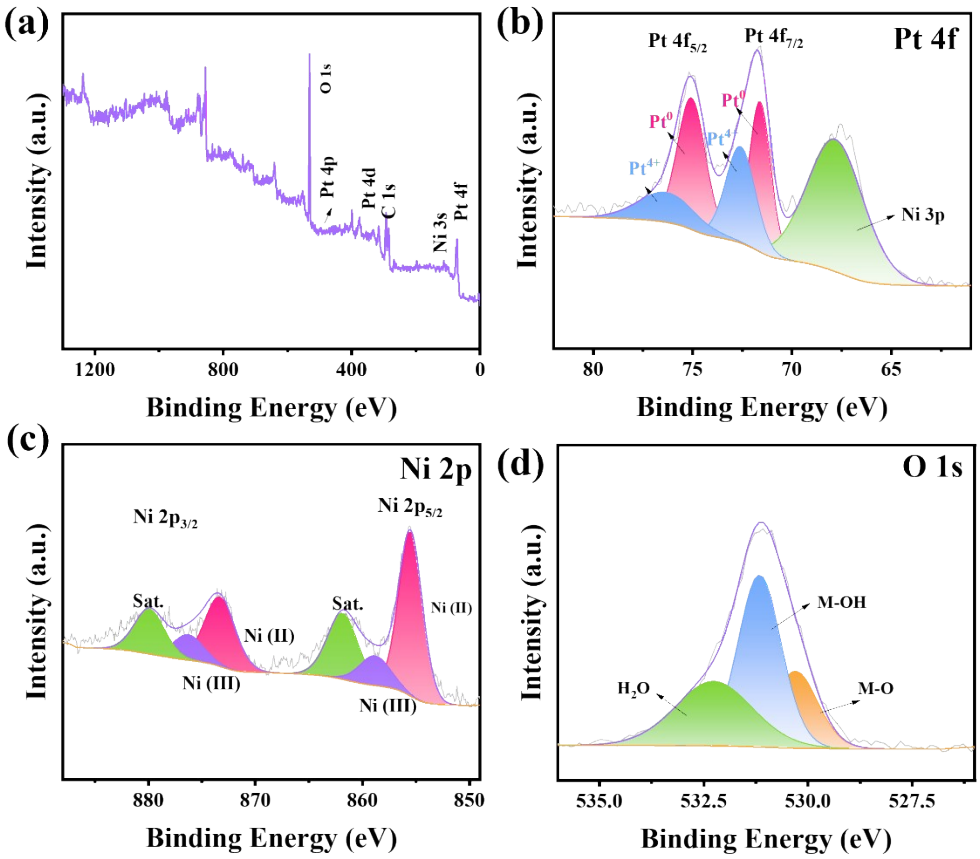

Fig. S12 XPS spectra of (a) full spectrum, (b) Pt 4f, (c) Ni 2p, and (d) O 1s of as-obtained samples after stability test for Pt/Ni(OH)$_2$/NF.

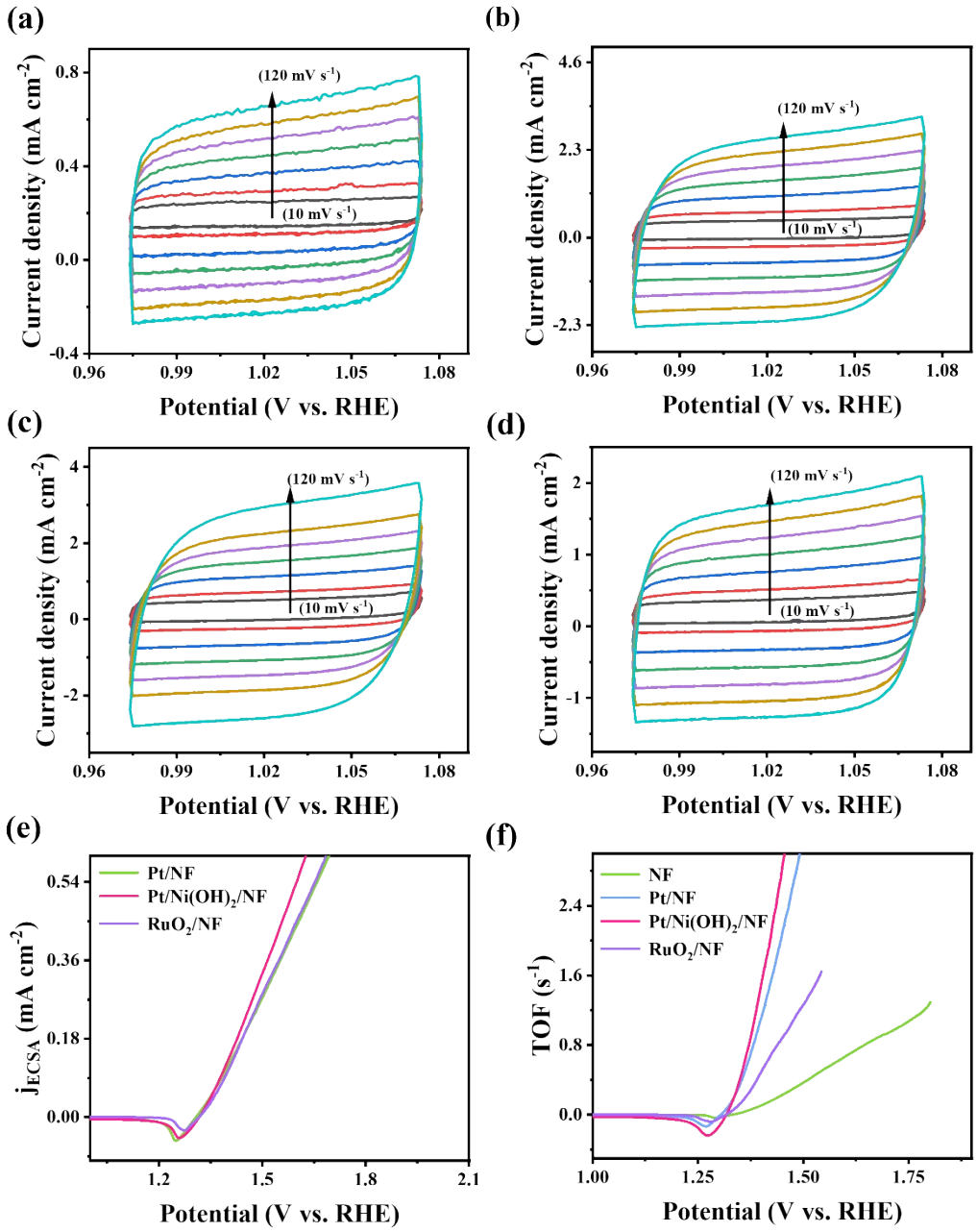

Fig. S13 The different sweep CV curves in the non-Faraday interval of (a) NF, (b) Pt/NF, (c) $Pt/Ni(OH)_2/NF$ and (d) Pt/C/NF. (e) ECSA normalized for the current density curves and (f) TOF values of the different samples in 1 M KOH + 0.5 M urea.

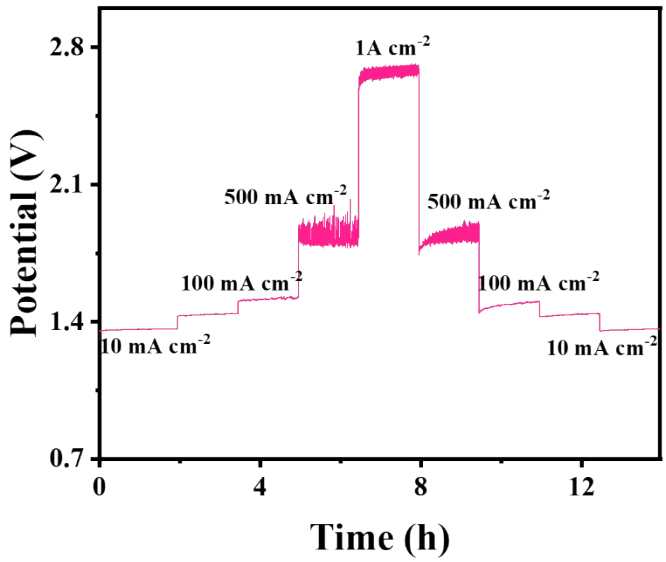

Fig. S14 The multi-step chronoamperometry tests of Pt/Ni(OH)$_2$/NF in UOR.

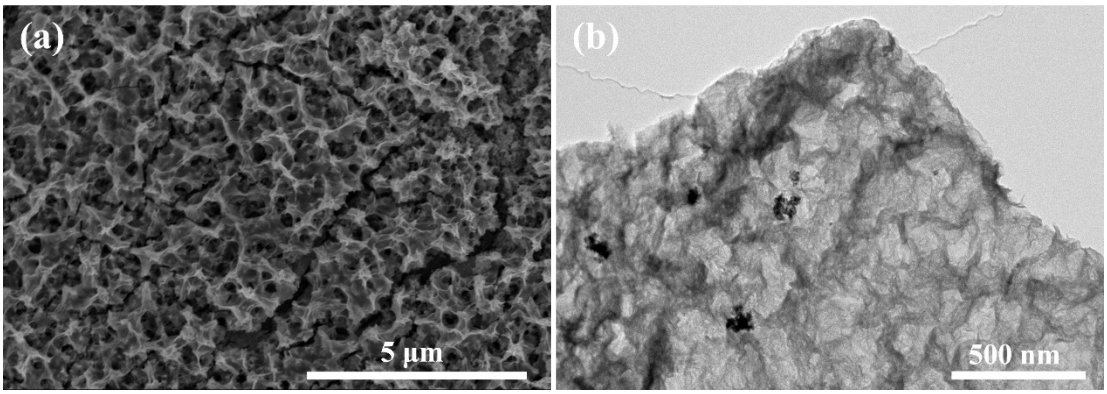

Fig. S15 (a) SEM diagram and (b) TEM diagram after stability test of Pt/$Ni(OH)_2$/NF in 1 M KOH + 0.5 M urea for UOR.

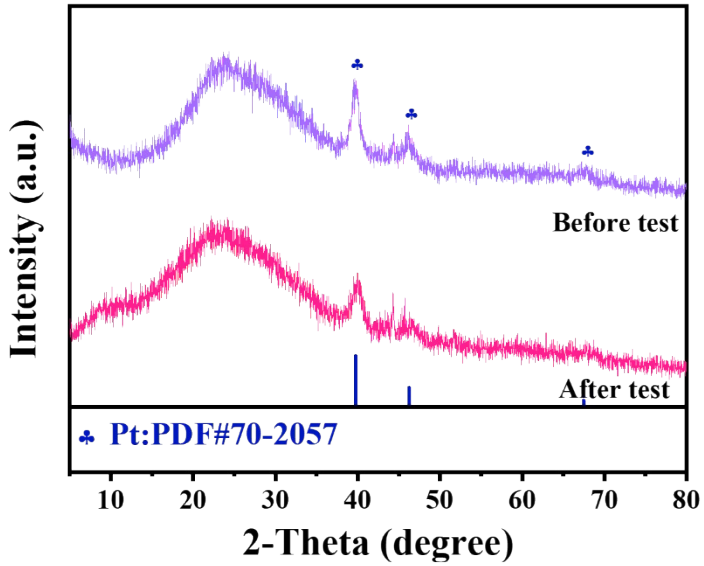

Fig. S16 XRD diagram before and after stability test for Pt/Ni(OH)$_2$/NF.

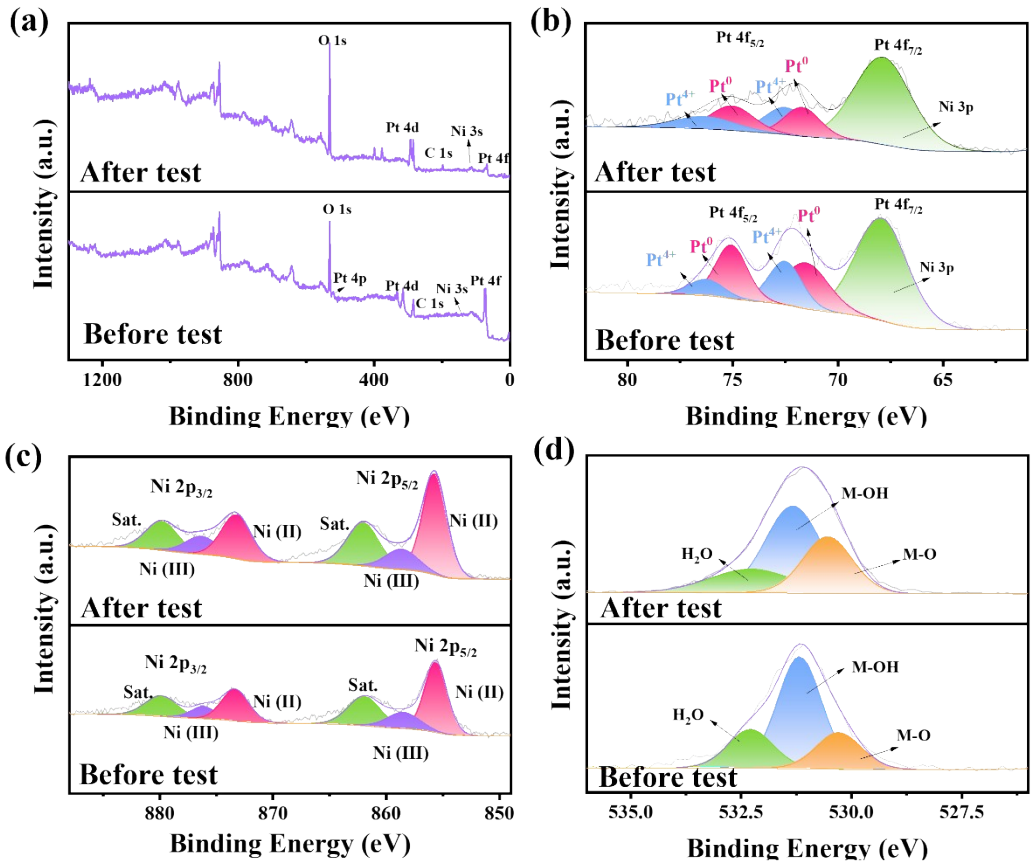

Fig. S17 XPS spectra of (a) full spectrum, (b) Pt 4f, (c) Ni 2p, and (d) O 1s of as-obtained samples after stability test for Pt/Ni(OH)$_2$/NF.

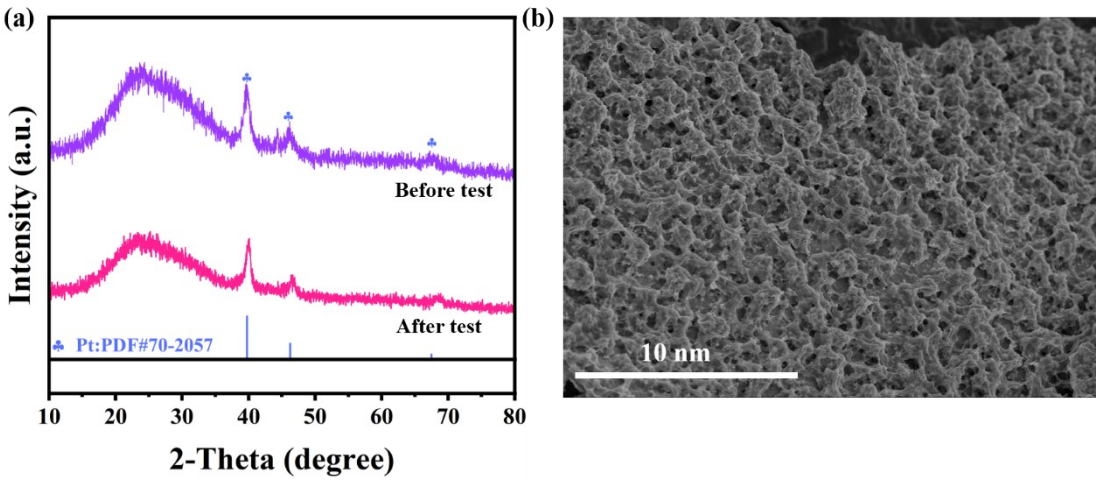

Fig. S18 (a) XRD patterns and (b) SEM diagram of Pt/Ni(OH)$_2$/NF after stability test for HER in 1 M KOH + 0.5 M urea + seawater.

Table S1. The content of Pt for $Pt/Ni(OH)_2/NF$ by ICP-OES test.

Sample	Pt content（wt%）
$Pt/Ni(OH)_2/NF$	0.59

Table S2. Comparison of the HER performance of $Pt/Ni(OH)_2/NF$ and the recently reported electrocatalysts

Catalyst	Electrolyte	Potential@current density（V@mA cm^{-2}）	Reference
$Pt/Ni(OH)_2/NF$	**1.0 M KOH**	**54 mV@100 mA cm^{-2}**	**This work**
Pt/Mo-NiOx/NMF	1.0 M KOH	62 mV@100 mA cm^{-2}	1
$Pt_{cluster}$-NiCoP@NF NWs	1.0 M KOH	65 mV@100 mA cm^{-2}	2
$Pt_2/Ni(OH)_2/NF$	1.0 M KOH	76 mV@100 mA cm^{-2}	3
Pt/FeOOH@NiFe LDHs	1.0 M KOH	85 mV@100 mA cm^{-2}	4
Pt/NiCo LDH	1.0 M KOH	91 mV@100 mA cm^{-2}	5
Fe_2O_3-Pt/NF	1.0 M KOH	94 mV@100 mA cm^{-2}	6
Pt-NiFe-P/NF	1.0 M KOH	97 mV@100 mA cm^{-2}	7
Pt-$Co(OH)_2$@$CoMoO_4$/NF	1.0 M KOH	100 mV@100 mA cm^{-2}	8
Pt-NiFe-MOF/NF	1.0 M KOH	125 mV@100 mA cm^{-2}	9
a/c-RuCoMoyOx/NF	1.0 M KOH	128 mV@100 mA cm^{-2}	10

Table S3. Comparison of UOR performance between $Pt/Ni(OH)_2/NF$ and recently reported electrocatalyst

Catalyst	Electrolyte	Potential@current density（V@mA cm^{-2}）	Reference
$Pt/Ni(OH)_2/NF$	**1.0 M KOH + 0.5 M urea**	**1.32 V@20 mA cm^{-2}** **1.34 V@50 mA cm^{-2}** **1.36 V@100 mA cm^{-2}**	**This work**
O-Ru-Ni_3N	1.0 M KOH + 0.33 M urea	1.34 V@10 mA cm^{-2} 1.38 V@50 mA cm^{-2}	11
Ru/FeOOH	1.0 M KOH + 0.33 M urea	1.41 V@10 mA cm^{-2}	12
Pt-NiFeP/NF	1.0 M KOH + 0.5 M urea	1.32 V@10 mA cm^{-2} 1.42 V@100 mA cm^{-2}	13
Pt/NiO/NF	1.0 M KOH + 0.5 M urea	1.33 V@10 mA cm^{-2} 1.43 V@100 mA cm^{-2}	14
Ir-NiFe-OH	1.0 M KOH + 0.33 M urea	1.33 V@10 mA cm^{-2} 1.38 V@100 mA cm^{-2}	15
Ir@Mn-NiOOH	1.0 M KOH + 0.5 M urea	1.33 V@10 mA cm^{-2}	16
Ru-NiO/Co_3O_4/NF	1.0 M KOH + 0.5 M urea	1.42 V@100 mA cm^{-2}	17

Table S4. Comparison of HER + UOR performance between $Pt/Ni(OH)_2/NF$ and recently reported electrocatalyst

Catalyst	Electrolyte	Potential@current density（V@mA cm^{-2}）	Reference
$Pt/Ni(OH)_2/NF$	**1.0 M KOH + 0.5 M urea**	**1.34 V@10 mA cm^{-2}** **1.43 V@50 mA cm^{-2}** **1.51 V@100 mA cm^{-2}**	**This work**
Pt-NiFeP/NF	1.0 M KOH + 0.5 M urea	1.41 V@100 mA cm^{-2}	13
Pt/NiO/NF	1.0 M KOH + 0.5 M urea	1.37 V@10 mA cm^{-2} 1.53 V@50 mA cm^{-2}	14
Ir-NiFe-OH	1.0 M KOH + 0.33 M urea	1.46 V@50 mA cm^{-2} 1.50 V@100 mA cm^{-2}	15
Pt-$Ni(OH)_2$@Ni-CNFs	1.0 M KOH + 0.5 M urea	1.40 V@10 mA cm^{-2} 1.54 V@50 mA cm^{-2}	18
Pt-NiS@Ni-CNFs	1.0 M KOH + 0.5 M urea	1.44 V@10 mA cm^{-2} 1.65 V@100 mA cm^{-2}	19
Ru-Ni_3N@NC	1.0 M KOH + 0.33 M urea	1.41 V@10 mA cm^{-2}	20

Reference

1 W. Liu, Y. Li, Y. Dou, N. Xu, J.J. Wang, J. Xu, C. Li, J. Liu, Light-driven assembly of Pt clusters on Mo-NiO_x nanosheets to achieve Pt/Mo-NiO_x hybrid with dense heterointerfaces and optimized charge redistribution for alkaline hydrogen evolution, *J. Colloid Interface Sci.*, 2024, **655**, 800-808.

2 D. Ren, D. Jiang, Y. Huang, Y. Jin, C. Zeng, K. Zhou, H. Wang, Well-defined ternary metal phosphide nanowires with stabilized Pt nanoclusters to boost alkaline hydrogen evolution reaction, *J. Colloid Interface Sci.*, 2024, **665**, 510-517.

3 J. Sun, Z. Zhang, X. Meng, Low-Pt supported on MOF-derived $Ni(OH)_2$ with highly-efficiently electrocatalytic seawater splitting at high current density, *Appl. Catal. B-Environ.*, 2023, **331**, 122703.

4 Y.C. Zhang, M. Zhao, J. Wu, Y. Wang, L. Zheng, F. Gu, J.J. Zou, J. Gao, X.D. Zhu, Construction of Pt single-atom and cluster/FeOOH synergistic active sites for efficient electrocatalytic hydrogen evolution reaction, *ACS Catal.*, 2024, **14**, 7867-7876.

5 J. Chen, Y. Wu, H. Zheng, M. Chen, H. Sun, T. Zhou, G. Na, D. Li, Q. Lu, B. Zi, T. He, J. Zhao, Y. Zhang, J. Zhang, F. Liu, H. Cui, Q. Liu, Facile room-temperature synthesis of Pt/NiCo LDH for enhanced hydrogen evolution reaction, *Int. J. Hydrogen Energy*, 2024, **72**, 41-48.

6 W. Xiao, Y. Zhang, C. Ke, Q. Zhao, F. Han, J. Guo, X. Yang, Constructing self-standing Fe_2O_3-Pt/NF nanoflowers with synergistic active sites for efficient electrocatalytic overall (sea) water splitting, *Nanoscale*, 2024, **16**, 22350-22359.

7 W. Zhang, X. Chen, J. Zhao, L. Niu, G. Wang, X. Wang, Manipulating electron redistribution in platinum for enhanced alkaline water splitting kinetics, Catal. Sci. Technol., 2024, 14, 3719-3727.

8 W.J. Li, R. Y. Fan, X. J. Tian, J. L. Tan, J. Y. Lv, N. Yu, B. Liu, Y. M. Chai, B. Dong, Ultralow-Pt-loading assisted by reconstruction of cobalt molybdate nanoarrays for enhanced hydrogen evolution reaction, *Int. J. Hydrogen Energy*, 2024, **56**, 837-843.

9 J. Yin, C. Wang, J. Li, S. Yu, Z. Wu, Y. Zhang, Y. Du, In situ electrodeposition of ultralow Pt into NiFe-metal-organic framework/nickel foam nanosheet arrays as a bifunctional catalyst for overall water splitting, *Inorg. Chem.*, 2024, **63**, 5167-5174.

10 J. Ren, Y. Du, Y. Wang, S. Zhao, B. Yang, B. Li, L. Wang, Modulating amorphous/crystalline heterogeneous interface in rucomoyox grown on nickel foam to achieve efficient overall water splitting, *Chem. Eng. J.*, 2023, **469**, 143993.

11 Y. H. Luo, H. C. Fu, X. H. Chen, B. J. Wang, B. Yang, N. B. Li, H. Q. Luo, Modulating adsorption energy on nickel nitride-supported ruthenium nanoparticles through in-situ electrochemical activation for urea-assisted alkaline hydrogen production, *J. Colloid Interface Sci.*, 2023, **652**, 1665-1672.

12 P. Zhao, Q. Liu, X. Yang, S. Yang, L. Chen, J. Zhu, Q. Zhang, Ru nanocrystals modified porous FeOOH nanostructures with open 3d interconnected architecture supported on nickel foam as high-performance electrocatalyst for oxygen evolution reaction and electrocatalytic urea oxidation, *J. Colloid Interface Sci.*, 2024, **673**, 49-59.

13 J. Miao, Q. L. Hong, P. Zhang, Z. F. Ren, A. C. Zhao, Y. H. Li, P. F. Wang, Y. Chen, Self-supported Pt nanoparticles-NiFeP nanosheets arrays nanohybrid with hydrophilic surface towards urea electrolysis, *Appl. Surf. Sci.*, 2024, **652**, 159276.

14 J. Li, Y. Lv, X. Wu, X. Guo, Z. Yang, J. Guo, T. Zhou, D. Jia, Surface confinement of sub-1 nm Pt nanoclusters on 1d/2d nio nanotubes/nanosheets as an effective electrocatalyst for urea-assisted

energy-saving hydrogen production, *Chin. J. Catal.*, 2025, **69**, 203-218.

15 X. Chen, J. Wan, J. Chai, L. Zhang, F. Zhang, Q. Zhang, L. Gu, L. Zheng, R. Yu, Nickel-iron in the second coordination shell boost single-atomic-site iridium catalysts for high-performance urea electrooxidation, *Nano Res.*, 2024, **17**, 3919-3926.

16 QP. Ngo, S. Prabhakaran, DH. Kim, BS. Kim, Rational design of ultrahigh-loading Ir single atoms on reconstructed mn horizontal line NiOOH for enhanced catalytic performance in urea-water electrolysis, *Small*, 2024, **20**, e2406786.

17 J.X. Li, Y. Lv, X.Y. Wu, R. Xue, Z.J. Yang, J.X. Guo, D.Z. Jia. Electronic and vacancy engineering of ruthenium doped hollow structured NiO/Co_3O_4 nanoreactors for low-barrier electrochemical urea-assisted energy-saving hydrogen production, *J. Colloid Interface Sci.*, 2024, **683**, 600-611.

18 M. Zhong, M. Xu, S. Ren, W. Li, C. Wang, M. Gao, X. Lu, Modulating the electronic structure of $Ni(OH)_2$ by coupling with low-content Pt for boosting the urea oxidation reaction enables significantly promoted energy-saving hydrogen production, *Energy Environ. Sci.*, 2024, **17**, 1984-1996.

19 M. Zhong, J. Yang, M. Xu, S. Ren, X. Chen, C. Wang, M. Gao, X. Lu, Significantly enhanced energy-saving H_2 production coupled with urea oxidation by low- and non-Pt anchored on NiS-based conductive nanofibers, *Small*, 2024, **20**, e2304782.

20 Y.B. Liu, D.B. Zheng, Y. Zhao, P. Shen, Y.X. Du, W.P. Xiao, Y.M. Du, Y.L. Fu, Z.X. Wu, L. Wang. Ru-doped 3D porous Ni_3N sphere as efficient Bi-functional electrocatalysts toward urea assisted water-splitting, *Int. J. Hydrogen Energy.*, 2022, **47**, 25081-25089.